THE JOURNAL OF BIOLOGICAL CHEMISTRY
Vol. 280, No. 7, Issue of February 18, pp. 6138–6148, 2005
Printed in U.S.A.

Accumulation of Free ADP-ribose from Mitochondria Mediates Oxidative Stress-induced Gating of TRPM2 Cation Channels*

Received for publication, October 7, 2004, and in revised form, November 18, 2004
Published, JBC Papers in Press, November 23, 2004, DOI 10.1074/jbc.M411446200

Anne-Laure Perraud‡§¶, Christina L. Takanishi‡§, Betty Shen‖, Shin Kang, Megan K. Smith‡, Carsten Schmitz‡, Heather M. Knowles‡‡, Dana Ferraris§§, Weixing Li§§, Jie Zhang§§, Barry L. Stoddard‖, and Andrew M. Scharenberg‡¶¶**

*From the ‡Department of Pediatrics, University of Washington and Children's Hospital and Regional Medical Center, Seattle, Washington 98195, the ‖Department of Basic Science, Fred Hutchinson Cancer Research Center, Seattle, Washington, 98109, the ‡‡National Jewish Medical and Research Center, Denver, Colorado 80206, §§Guilford Pharmaceuticals Inc., Baltimore, Maryland 21224, and **Genentech, South San Francisco, California 94080-4990*

TRPM2 is a member of the transient receptor potential melastatin-related (TRPM) family of cation channels, which possesses both ion channel and ADP-ribose hydrolase functions. TRPM2 has been shown to gate in response to oxidative and nitrosative stresses, but the mechanism through which TRPM2 gating is induced by these types of stimuli is not clear. Here we show through structure-guided mutagenesis that TRPM2 gating by ADP-ribose and both oxidative and nitrosative stresses requires an intact ADP-ribose binding cleft in the C-terminal nudix domain. We also show that oxidative/nitrosative stress-induced gating can be inhibited by pharmacological reagents predicted to inhibit NAD hydrolysis to ADP-ribose and by suppression of ADP-ribose accumulation by cytosolic or mitochondrial overexpression of an enzyme that specifically hydrolyzes ADP-ribose. Overall, our data are most consistent with a model of oxidative and nitrosative stress-induced TRPM2 activation in which mitochondria are induced to produce free ADP-ribose and release it to the cytosol, where its subsequent accumulation induces TRPM2 gating via interaction within a binding cleft in the C-terminal NUDT9-H domain of TRPM2.

Eukaryotic cells have been shown to react and adapt to conditions of oxidative stress produced by disulfide-inducing chemicals, reactive oxygen species (ROS),[1] or reactive nitrogen species (RNS) through a variety of redox-sensitive signaling pathways (variously reviewed in Refs. 1–12). Recently, the TRPM2 cation channel has been shown to undergo gating in response to oxidative or nitrosative stress occurring upon ROS or RNS exposure (13, 14). As TRPM2 is a novel dual function protein that possesses both ion channel and ADP-ribose hydrolase functions (15, 16), there has been great interest in understanding the molecular mechanisms through which oxidative and nitrosative stress activate TRPM2 channels, as well as the physiological role(s) of TRPM2-mediated ion fluxes and enzymatic activity in the context of cellular exposure to ROS and RNS.

TRPM2 is classified as a member of the transient receptor potential melastatin-related (TRPM) ion channel family based on the homology of its ≈600 amino acid N-terminal domain and ≈300 amino acid channel-forming domain to corresponding regions of other TRPM family members. The enzymatic function of TRPM is encoded by a C-terminal domain, designated the NUDT9-homology (NUDT9-H) domain, which is homologous to the NUDT9 ADP-ribose hydrolase (15, 17). *In vitro* studies of TRPM2 channel function using patch clamp techniques have suggested that ADP-ribose and NAD are both able to directly induce gating of full-length TRPM2 channels (14, 15, 18), and *in vitro* studies of the NUDT9-H domain demonstrate that it has a low level of ADP-ribose hydrolase activity and the apparent capacity to interact with NAD through its nudix hydrolase enzymatic motif (14, 15). However, there is a significant gap in understanding how the *in vitro* data on TRPM2 function relate to oxidative/nitrosative stress-induced TRPM2 gating in intact cells. First, because of technical difficulties with adenine nucleotide extraction, very few direct measurements of ADP-ribose levels have been made. Consequently, little is known about the metabolism of free ADP-ribose (see Ref. 19), particularly whether ADP-ribose could accumulate to the high 10s of μM levels required to induce TRPM2 gating (15). Second, although millimolar NAD concentrations have been shown to rapidly and reversibly induce TRPM2 gating in excised patch clamp studies, in whole cell patch clamp studies, NAD-induced TRPM2 activation takes much longer than either ADP-ribose-induced TRPM2 activation or the predicted time for diffusional equilibration of NAD with the cell interior (14, 18), observations which are difficult to reconcile with direct NAD-induced gating in a cellular context. In addition, the use of high concentrations of NAD brings with it the possibility of sufficient contaminating ADP-ribose or intra-experimental NAD hydrolysis to ADP-ribose to induce TRPM2 gating, precluding a definitive interpretation of such experiments as favoring NAD-induced gating over ADP-ribose-induced gating. Third, a putative splice variant of TRPM2 has been reported that is able to gate in response to high concentrations of peroxide (5 mM) but not in response to

* This work was supported by a National Institutes of Health Grant (to A. M. S.). The costs of publication of this article were defrayed in part by the payment of page charges. This article must therefore be hereby marked "*advertisement*" in accordance with 18 U.S.C. Section 1734 solely to indicate this fact.

§ Both authors contributed equally to this work.

¶ Present address: National Jewish Medical and Research Center, 1400 Jackson St., Denver, CO 80206.

¶¶ To whom correspondence should be addressed: Dept. of Pediatrics, University of Washington and Children's Hospital and Regional Medical Center, Health Science Bldg., RR309, 1959 N.E. Pacific Ave., Seattle, WA 98177. Tel.: 206-987-7314; Fax: 206-987-7324; E-mail: andrewms@u.washington.edu.

[1] The abbreviations used are: ROS, reactive oxygen species; RNS, reactive nitrogen species; TRPM, transient receptor potential melastatin; NUDT9-H, NUDT9-homology; MNNG, *N*-methyl-*N*′-nitro-*N*-nitrosoguanidine; HEK, human embryonic kidney; WT, wild type; MPT, mitochondrial permeability transition; mitNUDT9, mitochondrially targeted isoform of NUDT9; GFP, green fluorescent protein.

either NAD or ADP-ribose in whole cell patch clamp studies (13), indicating that under some circumstances TRPM2 gating in response to H_2O_2 may occur in a ligand-independent manner, although a recent report indicates that gating of this channel by peroxide is not consistently observed (20). In any case, the relevance of the behavior of this TRPM2 variant to full-length TRPM2 channels remains to be established. Because of the above issues, the molecular mechanisms through which oxidative/nitrosative stress induce TRPM2 gating in intact cells are presently controversial.

Here, we have undertaken a combination of structural, pharmacological, and cell biological approaches to explore in greater depth the mechanism through which oxidative/nitrosative stresses induce the activation of full-length TRPM2 channels. The data derived from our studies are not easily reconciled with NAD-induced or direct/membrane delimited models for oxidative/nitrosative stress-induced activation of full-length TRPM2 channels. Instead, they suggest that oxidative/nitrosative stress activates a mitochondrial biochemical pathway, which results in the production of ADP-ribose within the mitochondria, with the ADP-ribose thus produced being released to the cytosol where it acts as a diffusible second messenger to induce TRPM2 gating.

MATERIALS AND METHODS

Structural Modeling—The structural model of the NUDT9-H was produced by threading the sequence of NUDT9-H on to the refined structure of NUDT9 at 1.8 Å using MODELLER6v2 (21). The structure of the loop that replaces helix H5 in the NUDT9 structure was refined using the loop algorithm in the same program (22). A model of ADP-ribose was then docked into the NUDT9-H model followed by energy minimization using CNS (23).

Chemicals—Cyclosporin A, 5[H]-phenanthridin-6-one, H_2O_2, *N*-methyl-*N*′-nitro-*N*-nitrosoguanidine (MNNG), ADP-ribose, and all other standard salts and buffers used to make calcium imaging and patch clamp solutions content were obtained from Sigma. GPI-16539 was synthesized and purified as described previously (24).

Molecular Biology—A WT TRPM2 cDNA and TRPM2-expressing HEK-293 cells have been described previously (15). For generation of constitutive TRPM2-expressing HEK-293 cells, a TRPM2 expression construct with a glycine for serine substitution at position 1367 was placed into the pApuro plasmid with a modified cloning site to provide an N-terminal hemagglutinin-tag, with expression driven by the chicken β actin promotor, and was transfected into HEK-293 cells expressing the tetracycline suppressor under control of a CMV promotor. Single clones with various levels of TRPM2-dependent currents were grown out under puromycin selection. Clones with the highest level of TRPM2 expression (~10 nA of current elicited by 100 μM ADP-ribose under unbuffered calcium conditions) were then retransfected with various NUDT9 constructs under control of the pCDNA4/T0 plasmid and clones with inducible expression were selected under zeocin selection. The TRPM2(S1367G) channel behaved identically to WT TRPM2 channels in terms of both ADP-ribose induced gating by patch clamp and induction of fura-2 transient in response to ROS and RNS. Cytosolic NUDT9 and mitochondrial-targeted NUDT9 constructs have been described previously (17). Clones lacking detectable expression in the absence of doxycycline and with the highest level of doxycycline-induced expression were chosen for further analysis.

TRPM2 mutants were constructed by introducing a KpnI restriction site into our wild type TRPM2 sequence after position 1197, causing the amino acids sequence to change from . . . QTARALHWIVRTLRASGFSSEADVP . . . to . . . QTARALHWIVR*GT*TLRASGFSSEADVP . . . TRPM2 channels containing the introduced GT amino acids followed by the wild type NUDT9-H domain (without the S1367G substitution) behaved identically to wild type TRPM2 channels (data not shown). Point mutations were then made in the isolated NUDT9-H domain and spliced onto the rest of the TRPM2 sequence by subcloning using the KpnI site. The predicted amino acids sequences of all constructs were verified by DNA sequencing. NUDT9 mutants were produced using QuikChange to introduce mutations into the indicated residues as described previously (17).

Immunoblotting—Using stable HEK cell lines with doxycycline-inducible expression of the indicated channels, 10^{-7} cells were induced and plated for 48 h under conditions identical to those utilized for imaging and patch clamp experiments. The cells were then harvested, and surface-labeled with biotin. After inactivation of residual biotinylation reagent, the cells were then lysed and immunoprecipitated with anti-FLAG antibody. The anti-FLAG immunoprecipitates were washed extensively and analyzed by Western blotting, first with streptavidin-horseradish peroxidase immunoblotting to detect surface expressed protein, followed by a stripping of the membrane and anti-FLAG immunoblotting to detect total expressed protein using standard luminal-based techniques.

Cell Culture—HEK-293 cells transfected with the FLAG-human TRPM2/pCDNA4/TO construct were grown on glass coverslips with Dulbecco's modified Eagle's medium supplemented with 10% fetal bovine serum, blasticidin (5 μg/ml), and zeocin (0.4 mg/ml) for 48 h prior to imaging and patch clamp experiments. TRPM2 expression was induced by adding 1 μg/ml doxycycline to the culture medium. Stable TRPM2 cells with inducible NUDT9 expression were grown in culture, and NUDT9 expression was induced in a manner identical to that used for the inducible TRPM2 cell lines.

Calcium Imaging—Changes in cytosolic calcium were monitored using changes in fura-2 fluorescence measured using a TILL Photonics imaging system IV and otherwise standard methods. Briefly, cells were plated on 25 mM circular coverslips 48 h prior to analysis and either left untreated or treated with 1 μg/ml of doxycycline. The coverslips were then placed at room temperature in a microscope chamber and imaged by exposure every 2 or 5 s to 340/380 nm excitation accompanied by monitoring 510 nm emission light for the period of time indicated in each panel. The indicated stimuli were added to the chamber manually at the time indicated in the panels. Bath solution contained 135 mM NaCl, 5 mM KCl, 1 mM $MgCl_2$, 1 mM $CaCl_2$, 5.6 mM glucose, 10 mM Hepes, and 0.1% bovine serum albumin.

It is likely that other cation channels may contribute a portion of calcium entering in response to exposure of intact cells to larger concentrations of ROS and that this may contribute to the small calcium transients occurring in the absence of TRPM2. Therefore, whenever appropriate, we attempted to choose conditions such that any calcium entering through such other channels was either minimized or insufficient to induce an alteration in cytosolic calcium concentration (*e.g.* the use 100 μM H_2O_2, or the use of 100 μM MNNG, each of which generally produced only a small alteration or no significant alteration of cytosolic calcium in cells lacking TRPM2 expression, see Fig. 1). A higher concentration of H_2O_2 was used to generate maximal calcium responses in all TRPM2 mutant-expressing cell lines and was also used to help evaluate whether a general antioxidant effect of a pharmacological treatment could be contributing to the observed inhibition of the TRPM2-dependent component of a response. Note that although 1 mM or higher concentrations of H_2O_2 induced significant cell toxicity in the absence of TRPM2, treatment of cells with 100 μM H_2O_2 produced little apparent toxicity even after 24 h of exposure (data not shown).

Patch Clamp—Whole cell patch clamp experiments were performed at 21–25 °C 18–24 h post-induction, using cells grown on glass coverslips and kept in a standard modified Ringer's solution of the following composition, NaCl 145 mM, KCl 2.8 mM, CsCl 10 mM, $CaCl_2$ 1 mM, $MgCl_2$ 2 mM, glucose 10 mM, and Hepes·NaOH 10 mM, pH 7.2. Intracellular pipette-filling solutions contained Cs-glutamate 145 mM, NaCl 8 mM, $MgCl_2$ 1 mM, Cs-EGTA 10 mM, pH 7.2, adjusted with CsOH, or Cs-glutamate 145 mM, NaCl 8 mM, $MgCl_2$ 1 mM, pH 7.2, adjusted with CsOH. The amount of ADP-ribose included in the patch pipette is indicated in the legend associated with each patch clamp experiment figure. High-resolution current recordings were acquired by a computer-based patch clamp amplifier system (EPC-9, HEKA, Lambrecht, Germany). Immediately following establishment of the whole cell configuration, voltage ramps of 50-ms duration spanning the voltage range of −100 to +100 mV were delivered from a holding potential of 0 mV at a rate of 0.5 Hz over a period of 200–400 s. All voltages were corrected for a liquid junction potential of 10 mV between external and internal solutions when internal solutions contained glutamate. Currents were filtered at 2.3 kHz and digitized at 100-μs intervals. Capacitative currents and series resistance were determined and corrected before each voltage ramp using the automatic capacitance compensation of the EPC-9. The low-resolution temporal development of currents at a given potential was extracted from individual ramp current records by measuring the current amplitudes at voltages of −80 or +80 mV.

Each inducible cell line was evaluated in the presence and absence of doxycycline induction. In the absence of doxycycline induction, in no case were significant TRPM2-like currents ever observed, *e.g.* baseline currents in untransfected HEK-293 cells at −80 mV were at most 5–10 pA inward, and at +80 mV, 10–15 pA outward and baseline currents in all transfected cell lines were not distinguishable from those in the

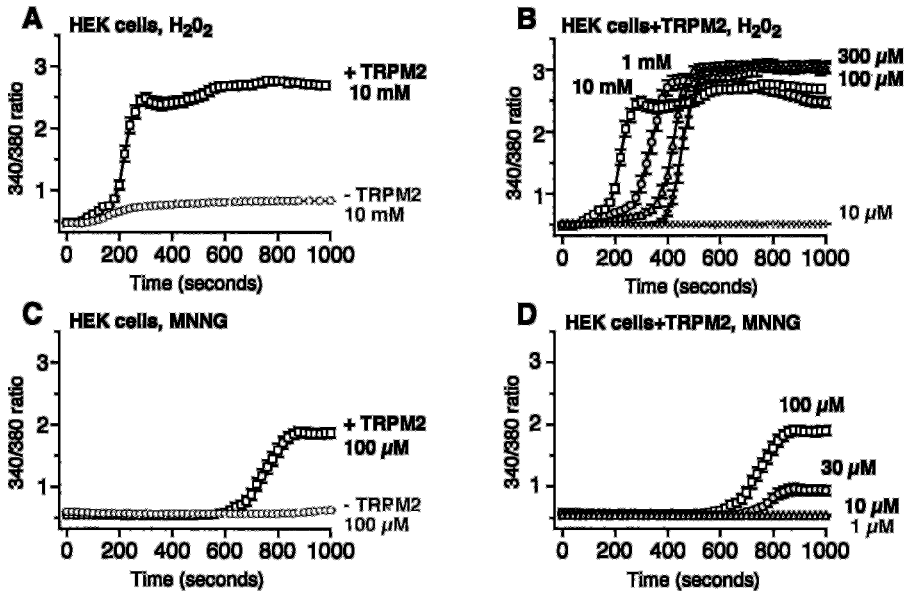

FIG. 1. **Activation of TRPM2-dependent calcium entry by ROS and RNS.** *A* and *B*, H_2O_2-mediated activation of TRPM2. *A*, calcium transients evoked by 10 mM H_2O_2 in the absence of doxycycline (*gray trace with circles*) or 36 h after induction of TRPM2 expression with doxycycline (*black trace with squares*). Note shoulder of transient in TRPM2-expressing cells, which represents a response attributable to calcium signaling pathways activated in the absence of TRPM2 expression. *B*, dose-response curve for H_2O_2-induced calcium transients in TRPM2-expressing HEK-293 cells. Note that shoulder response indicating activation of endogenous calcium signaling pathways and other oxidant-dependent events decreases with decreasing H_2O_2 concentrations and is absent when a concentration of 100 μM H_2O_2 is used. The lowest trace (10 μM) showing no TRPM2 activation is shown in *light gray*. *C* and *D*, MNNG-mediated activation of TRPM2. *C*, calcium transients evoked by 100 μM of the nitrosothiol donor MNNG (42, 57) in the absence of doxycycline (*gray trace with circles*) or 36 h after induction of TRPM2 expression with doxycycline (*black trace with squares*). Note the near absence of a response in uninduced cells and the absence of a shoulder of the transient in TRPM2-expressing cells. *D*, dose-response curve for MNNG-induced calcium transients in TRPM2-expressing HEK-293 cells. The lowest trace (1 μM) showing no TRPM2 activation is shown in *light gray*.

untransfected cells. This would place an upper limit of 1–2 channels on the number of surface-expressed TRPM2 channels in uninduced cells. Under the recording conditions used, we observed no significant evolution of other cation currents known to be present in HEK-293 cells, including TRPM7-like currents (data not shown).

RESULTS

In the course of investigations of the effects of various types of oxidative/nitrosative stress on TRPM2 gating, we noted that TRPM2-dependent calcium transients are activated in response to cellular exposure to a variety of forms of ROS and RNS (Fig. 1), including exposure to MNNG, which in addition to inducing nitrosative stress has been shown to produce markedly diminished NAD levels in HEK cells over a time course in which we observed sustained TRPM2 gating (25). Furthermore, disulfide stress induced by the disulfide-inducing reagent diamide did not initiate TRPM2-dependent calcium transients (data not shown), indicating that the pathway leading to TRPM2 activation most likely involves oxidative/nitrosative modification of one or more protein thiol group(s) (2, 26, 27), as opposed to a more general effect on cellular redox balance. These observations are difficult to reconcile with a proposed model of TRPM2 activation involving accumulation of NAD because of generalized adenine nucleotide oxidation and its agonistic binding to the NUDT9-H domain (14), and suggested to us that oxidative/nitrosative stress-mediated TRPM2 activation must involve an alternative mechanism.

As an initial step toward obtaining insight into potential alternative TRPM2 gating mechanisms, we focused on obtaining an improved understanding of NUDT9-H domain interactions with NAD and ADP-ribose by using the NUDT9 crystal structure to construct a structural model of the NUDT9-H domain of TRPM2 (Fig. 2*A*, alignment of NUDT9 and NUDT9-H sequences is shown). As illustrated in Fig. 2*B*, this model possesses an apparent binding cleft similar to that previously identified in NUDT9 (28). Docking of ADP-ribose into this binding cleft results in a predicted mode of binding very similar to that of ADP-ribose with NUDT9, with conservation of three residues in closest proximity to ADP-ribose, Asp^{1431} and His^{1488} (corresponding to Asp^{271} and His^{324} of NUDT9) interacting with the ribose ring and Asn^{1345} (corresponding to Asn^{168} of NUDT9) interacting with the adenine ring (28). An important prediction of this model is that the non-nucleoside ribose ring of ADP-ribose binds into a pocket that is incapable of accommodating an additional bulky nicotinamide group, as would be required for NAD to bind the NUDT9-H in a manner similar to ADP-ribose (Fig. 2*B*). This prediction is supported by our previous observation that the NUDT9-H has a small amount of hydrolase activity toward ADP-ribose but not NAD, consistent with the former but not the latter having access to the NUDT9-H binding cleft/active site (15). This prediction also has the important implication that neither direct binding nor agonistic activation of TRPM2 by NAD would be likely to occur through an interaction within the binding cleft identified in our model.

To experimentally assess whether the predicted NUDT9-H binding cleft has a requisite role in either ADP-ribose-induced or oxidative/nitrosative stress-induced TRPM2 gating, we used the NUDT9-H structural model to identify residues within the predicted binding cleft, which would not be likely to affect global NUDT9-H folding or expression, but which could potentially influence the function of the NUDT9-H domain. Of the three residues in closest contact with the docked ADP-ribose (Asn^{1345}, His^{1488}, and Asp^{1431}), all were within conserved secondary structures (β sheet B7, helix H7, and the highly conserved and deeply buried L5 loop, respectively (Fig. 3*A*, see also Ref. 28), likely to be important for NUDT9-H folding or stability and were therefore projected as poor candidates for mutagenesis. Consequently, we focused on introducing mutations into nudix motif residues within the binding cleft, which our homology model suggested would not contribute interactions

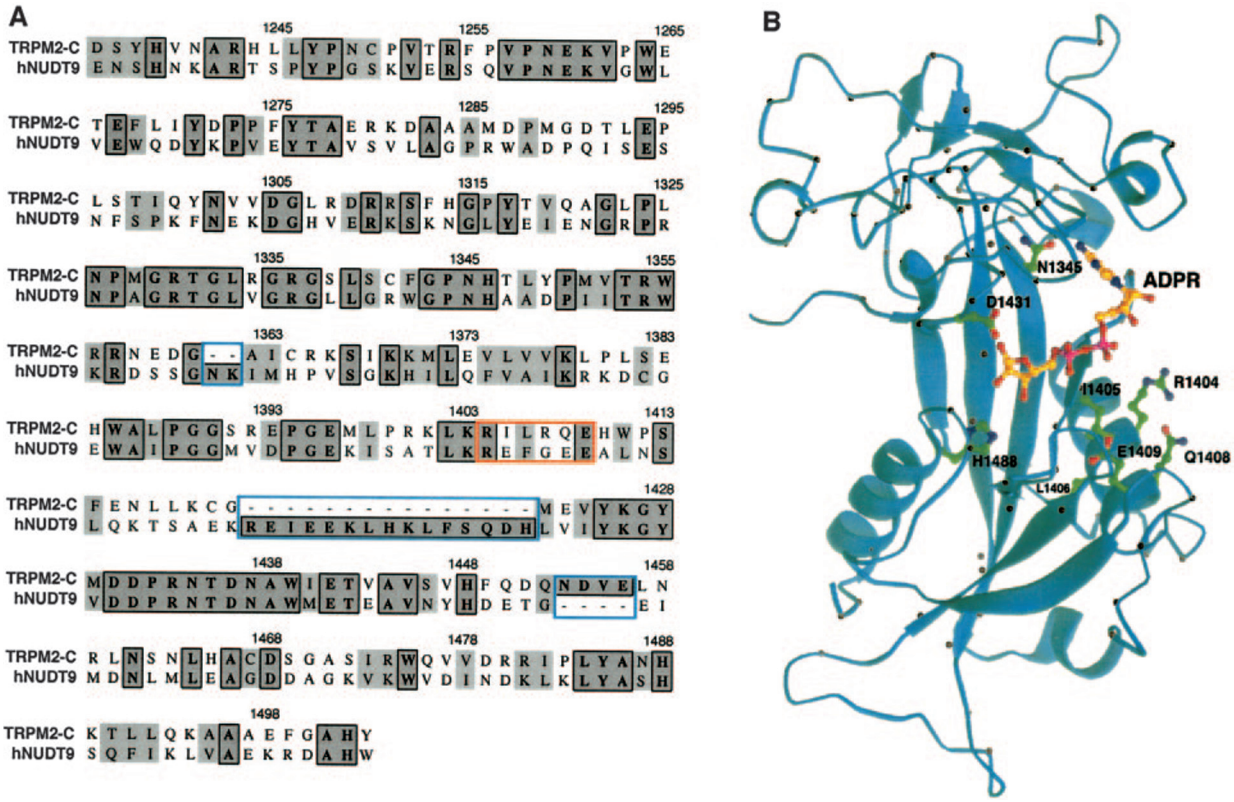

FIG. 2. **Homology model of the NUDT9-H.** *A*, ClustalW alignment of human NUDT9 with the NUDT9-H. The amino acid sequences of NUDT9 and the NUDT9-H closely correspond (*dark shading* denotes identities, *lighter shading* denotes similarities). Two deletions (2 residues and 15 residues) and a single 4 amino acid insertion in TRPM2 are required to produce alignment of all other conserved residues in the two sequences (the deletions and insertion are *boxed* in *blue*). This close correspondence supports the concept that an energy-minimized model of the NUDT9-H based on the NUDT9 structure provides a useful approximation of the actual NUDT9-H three-dimensional structure. Nudix motif active site residues subjected to site-directed mutagenesis in Fig. 3 are *boxed* in *red* in the alignment, and *colored* in the *ribbon diagram* at right. Positions of identities are indicated with *black spheres* in the structural model (*right panel*). *B*, ribbon diagram of the NUDT9-H docked with ADP-ribose. Note that the 15-residue deletion in the NUDT9-H relative to NUDT9 comprises a NUDT9 surface helix whose absence would not obviously affect folding of the NUDT9-H, whereas the residues inserted in the NUDT9-H are predicted to lie in solvent-exposed loops, which would also be unlikely to significantly affect folding of the NUDT9-H. *Black spheres* denote resides identical between NUDT9 and the NUDT9-H

likely to be required for folding or stability of the overall NUDT9-H domain (Fig. 3*A*, residues enclosed in *red oval* (28)). Six TRPM2 constructs with individual or selected combinations of amino acid changes in the nudix motif were transfected under control of a doxycycline-controlled promotor into HEK-293 cells, and stable cell lines with inducible protein expression were isolated. The resulting cell lines were induced with doxycycline and analyzed for their capacity to support an enhanced H_2O_2-mediated calcium transient using fura-2 imaging, and for the presence of ADP-ribose-dependent currents by whole cell patch clamp (Fig. 3*B*, *left plots* show calcium transients; *right plots* show ADP-ribose-dependent current evolution; point mutant channels that did not produce ADP-ribose-dependent currents or a calcium transient were analyzed biochemically for surface expression, in *C*). Two important observations emerged from these experiments. First, enzymatic activity of the NUDT9-H is apparently not required for channel gating, as the TRPM2 RILRKK mutant, which possesses mutations in two nudix motif residues absolutely required for NUDT9 enzymatic activity (17), is able to support both ADP-ribose-dependent channel gating and H_2O_2-induced calcium transients. Second, although idiosyncratic effects of a mutational approach cannot be excluded, TRPM2 channel gating via either ADP-ribose or oxidant stress exposure appears to occur through a common mechanism linked to the NUDT9-H binding cleft, as two mutant point channels (QILRQE and REFREE mutants) that lost the capacity for ADP-ribose-induced gating also lost the capacity for oxidant-induced gating despite being appropriately surface-expressed (Fig. 3*C*).

The observation that two point mutant TRPM2 channels had correlated behavior in terms of their gating responses to ADP-ribose and oxidative stress is in contrast to the initially reported behavior of a TRPM2 deletion mutant missing amino acids 1292–1325 (hereafter designated TRPM2-Δ(1292–1325)) (13). Despite the predicted destruction of its ADP-ribose binding cleft and resulting loss of capacity to gate in response to ADP-ribose, this mutant has been reported to retain the capacity to gate in response to 5 mM peroxide (13). To better understand the behavior of the TRPM2-Δ(1292–1325) channel, we reproduced the TRPM2-Δ(1292–1325) deletion mutation on the same TRPM2 backbone as our mutants, produced a stable inducible cell line expressing it, and analyzed the capacity of this cell line to support oxidative stress-induced calcium transients and ADP-ribose-induced currents after doxycycline induction. In fura-2 calcium experiments, we observed no detectable oxidative stress-induced calcium transients using 1 mM H_2O_2 (Fig. 3, *bottom right panel*, nor with 10 mM H_2O_2, data not shown), and 100 μM–1 mM MNNG (data not shown). Whole cell patch clamp experiments also revealed no detectable ADP-ribose-induced gating using up to 10 mM ADP-ribose in the patch pipette (Fig. 3, *bottom right panel*). Unfortunately, the determination of whether this mutant lacks detectable channel function because of difficulties with surface expression *versus* difficulties with ADP-ribose binding is not possible, as the mutant protein does not express as well as WT TRPM2, pre-

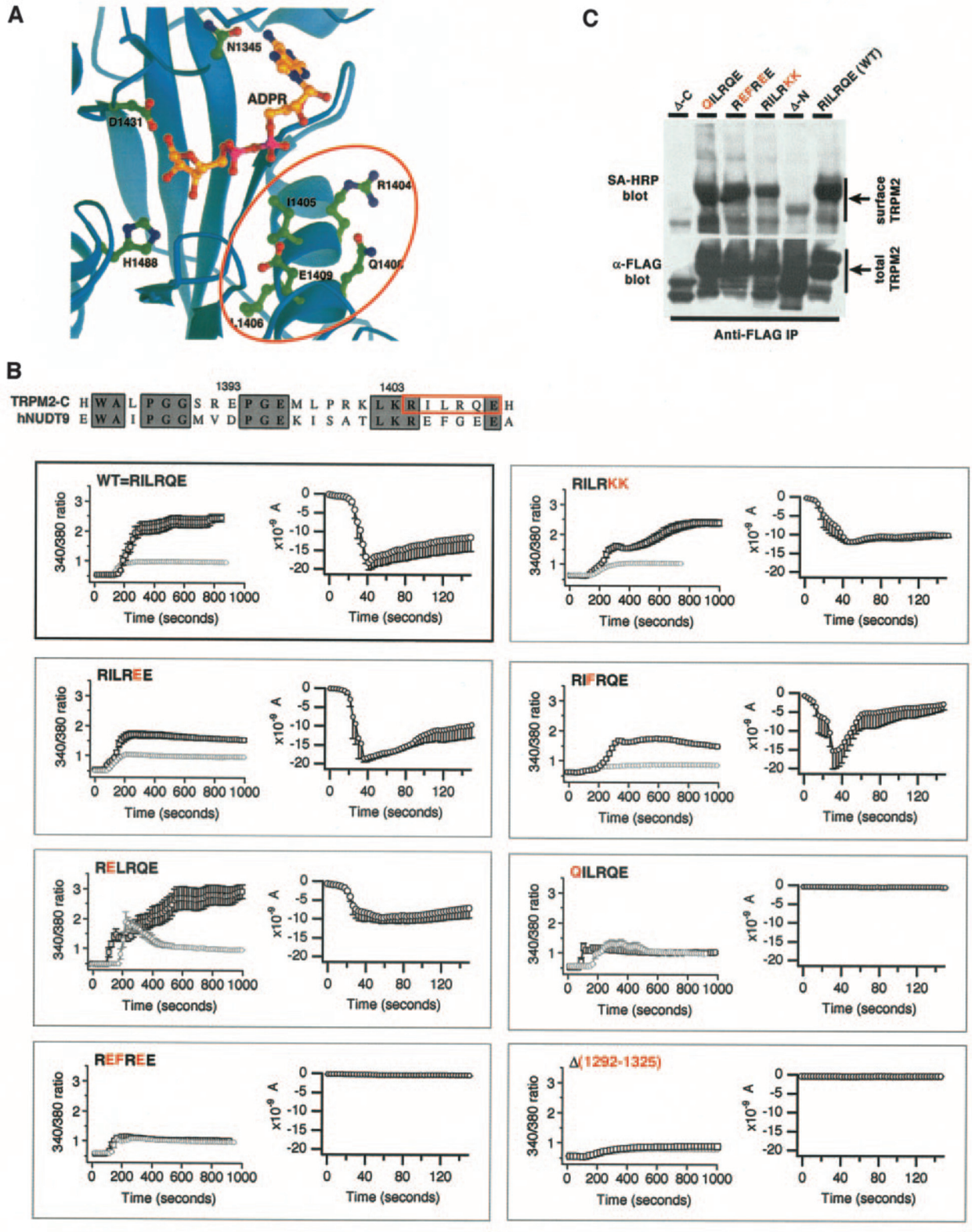

FIG. 3. **Characterization of NUDT9-H binding cleft mutants.** *A* and *B*, summary of gating behavior of NUDT9-H binding cleft point mutants. *A*, close up view of putative NUDT9-H binding cleft, indicating the position of the mutated residues (inside *red oval*) in relation to the bound ADP-ribose. NUDT9-H nudix motif residues subjected to mutagenesis are also *boxed* in *red* in both Fig. 2 and in the NUDT9-H/NUDT9 alignment in *B*. *B*, characterization of mutant TRPM2 channels: The alignment shows the nudix boxes of TRPM2 and NUDT9. Each TRPM2 mutant (the residues which are altered in each mutant are denoted in *red*) was analyzed for the presence of 1) calcium transients induced by 1 mM H_2O_2 (*left panel*) in the absence of doxycycline (*gray trace*) or after a 36-h induction with doxycycline (*black trace*). The calcium transients occurring in response to 1 mM H_2O_2 are presented, as this H_2O_2 was required to produce maximal amplitudes of TRPM2-mediated calcium transients in some cell lines, and 2) whole cell patch clamp currents elicited by 100 μM ADP-ribose under unbuffered calcium conditions in doxycycline-induced cells (*right panel*). Note that ADP-ribose-induced currents all possessed linear I/V relationships characteristic of TRPM2 (data not shown). No significant currents with TRPM2-like biophysical characteristics were induced by ADP-ribose in the absence of doxycycline induction in any of the cell lines analyzed (data not shown), consistent with our past experience that Tet suppressor protein-based inducible expression systems maintain very tight control over protein expression levels (15). *C*, biochemical analysis of surface expression of selected TRPM2 channels. 10^{-7} HEK cells

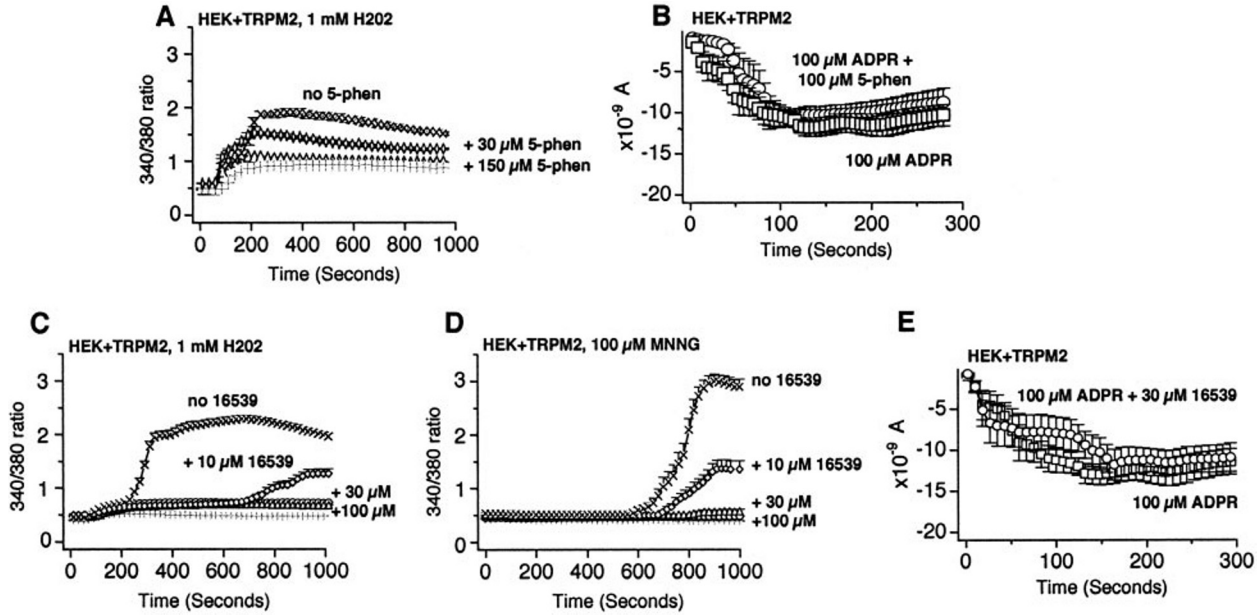

FIG. 4. **Inhibition of oxidant-induced TRPM2-dependent calcium transients by small molecule structural mimics of nicotinamide.** *A* and *B*, inhibition of TRPM2 gating by 5[H]-phenanthridin-6-one. *A*, dose-dependent inhibition by 5[H]-phenanthridin-6-one of calcium transients elicited by 1 mM H_2O_2 in TRPM2-expressing HEK cells. Note that the TRPM2-independent shoulder component of the calcium transient induced by 1 mM H_2O_2 is not affected by 5[H]-phenanthridin-6-one (the *light gray trace* marked by + is the calcium transient induced in the absence of TRPM2 expression). *B*, 100 μM 5[H]-phenanthridin-6-one does not affect TRPM2-dependent whole cell currents elicited by 100 μM ADP-ribose under unbuffered calcium conditions. *Squares* are currents elicited by 100 μM ADP-ribose in the absence of 100 μM 5[H]-phenanthridin-6-one; *circles* are the currents elicited in the presence of 100 μM 5[H]-phenanthridin-6-one. *C–E*, inhibition of TRPM2 gating by GPI16539. *C*, dose response for inhibition by GPI16539 of calcium transients elicited by 1 mM H_2O_2 in TRPM2-expressing HEK cells. Note that the TRPM2-independent shoulder component of the calcium transient is not affected by GPI16539 (the l*ight gray trace* marked by + is the calcium transient induced in the absence of TRPM2 expression). *D*, dose response for inhibition by GPI16539 of calcium transients elicited by 100 μM MNNG in TRPM2-expressing HEK cells (the *light gray trace* marked by + is the calcium transient induced in the absence of TRPM2 expression). *E*, 30 μM GPI16539 does not block TRPM2-dependent whole cell currents elicited by 100 μM ADP-ribose under unbuffered calcium conditions. *Squares* are currents elicited by 100 μM ADP-ribose in the absence of 100 μM 5[H]-phenanthridin-6-one; *circles* are the currents elicited in the presence of 100 μM 5[H]-phenanthridin-6-one.

cluding meaningful analysis of its surface expression via biochemical approaches. Although the reasons for the discrepancy between our results and those of the original Wehage *et al.* (13) manuscript are unclear, it is notable that the same group has also recently reported that H_2O_2-mediated activation of WT or mutant TRPM2 channels is not consistently evocable, a result strongly weighing against the existence of a direct mechanism of H_2O_2-mediated TRPM2 gating (20). Taking our TRPM2-Δ(1292–1325) data together with the reported inconsistency of direct H_2O_2 gating of even WT TRPM2 (20), TRPM2-Δ(1292–1325) channels can be concluded to lack the capacity to gate directly in response to either H_2O_2 or ADP-ribose, behavior in accord with the correlated oxidant/ADP-ribose gating we observed in our set of TRPM2 point mutant channels.

The observation that oxidant and ADP-ribose gating of TRPM2 channels are linked could be most simply explained if oxidative/nitrosative stress cause cells to produce and accumulate free ADP-ribose, with the ADP-ribose acting as an intracellular ligand to induce TRPM2 gating. To test this possibility, we chose to exploit a bottleneck in ADP-ribose metabolism; the production of ADP-ribose is thought to occur essentially entirely through hydrolysis of the glycosyl bond between nicotinamide and the non-nucleoside ribose ring of NAD (29–31). Consequently, any mechanism involved in producing ADP-ribose likely involves a protein that interacts with and hydrolyzes NAD. A search for potential pharmacological reagents capable of acting as structural analogues of NAD revealed several classes of compounds that inhibit the poly(ADP-ribose)-polymerase family of enzymes through their structural mimicry of the nicotinamide head group of NAD (32, 33), and which have been shown to prevent MNNG-induced NAD hydrolysis and resulting NAD depletion (25). We tested the effect of two such compounds, 5[H]-phenanthridin-6-one and 2-(4-methylpiperazin-1-yl)-5H-benzo[c](1,5)naphthyridin-6-one (24) (henceforth designated GPI16539), on H_2O_2 and MNNG-mediated gating of TRPM2 (Fig. 4). As can be seen, both compounds dose-dependently inhibited TRPM2 activation. Importantly, neither compound influenced direct ADP-ribose-dependent gating of TRPM2 in whole cell patch clamp experiments, indicating that the capacity to inhibit oxidative/nitrosative stress-mediated TRPM2 gating is not through a direct effect on TRPM2. Also, neither compound exhibited significant effects on TRPM2-independent components of oxidant-induced calcium transients, indicating that their capacity to inhibit oxidative/nitrosative stress-mediated TRPM2 gating cannot be explained as the result of strong general antioxidant effects. The ability of two distinct molecules to block oxidative/nitrosative stress-mediated TRPM2 gating independent of a direct effect

were induced to express the indicated channel, subjected to surface labeling with biotin, and analyzed by streptavidin-horseradish peroxidase (*SA-HRP*) immunoblotting to detect surface-expressed protein, and anti-FLAG immunoblotting to detect total protein. Δ-*N* is a mutant NUDT9-channel lacking the first 28 amino acids of the human TRPM2 sequence; Δ-*C* is a mutant TRPM2 channel lacking the entire nudix domain (residues 1236–1503 of human TRPM2). Neither of these deletion mutant channels exhibits a detectable ADP-ribose gating via patch clamp or oxidant gating via fura-2 measurements (data not shown) and function as negative controls to illustrate that a subset of non-functional channels have markedly decreased surface labeling, which plausibly accounts for their lack of function. In contrast, the QILRQE, REFREE, and RILRKK channels label to a similar extent as wild type RILRQE channels.

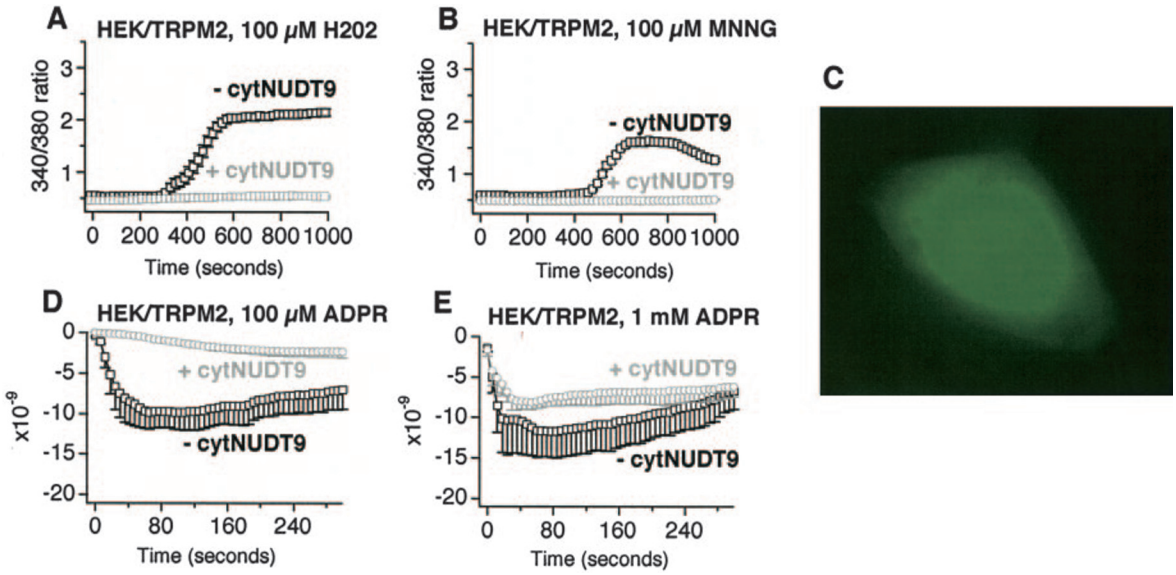

FIG. 5. **Overexpression of ADPRase activity in the cytosol suppresses TRPM2-dependent calcium transients induced by ROS or RNS.** *A* and *B*, influence of cytNUDT9 on ROS/RNS-induced TRPM2-dependent calcium transients *A*, expression of cytNUDT9 suppresses H_2O_2-induced TRPM2-activation. Shown are calcium transients induced by 100 μM H_2O_2 after induction of cytNUDT9 expression with doxycycline (*gray traces* with *circles*) or in the absence of cytNUDT9 expression (*black traces* with *squares*). *B*, expression of cytNUDT9 suppresses MNNG-induced TRPM2 activation. Shown are calcium transients induced by 100 μM MNNG after induction of cytNUDT9 expression with doxycycline (*gray traces* with *circles*) or in the absence of cytNUDT9 expression (*black traces* with *squares*). These studies were performed with 100 μM H_2O_2 and 100 μM MNNG as these stimulus concentrations induced no detectable toxicity over the course of a 1000-s imaging period as assessed by trypan blue staining (data not shown). *C*, subcellular distribution of cytNUDT9 tagged C-terminally with GFP. HEK-293 cells expressing TRPM2 were induced to express a cytNUDT9-GFP fusion protein for 36 h. GFP fluorescence was imaged using 480 nm excitation and detection of 510–530 nm emission light on a Zeiss Axiovert 100 microscope. *D* and *E*, influence of cytNUDT9 on direct gating of TRPM2 with ADP-ribose. *D*, expression of cytNUDT9 suppresses whole cell patch clamp currents elicited by 100 μM ADP-ribose under unbuffered calcium conditions. Shown are currents elicited by 100 μM ADP-ribose after induction of cytNUDT9 expression with doxycycline (*gray traces* with *circles*) or in the absence of cytNUDT9 expression (*black traces* with *squares*). *E*, after cytNUDT9 expression, whole cell patch clamp currents elicited by 1 mM ADP-ribose under unbuffered calcium conditions exhibit similar latency to activation and peak current development to those recorded in the absence of cytNUDT9 expression. Shown are currents elicited by 1 mM ADP-ribose after induction of cytNUDT9 expression with doxycycline (*gray traces* with *circles*) or in the absence of cytNUDT9 expression (*black traces* with *squares*). Note the more rapid current evolution in both uninduced and induced conditions relative to the use of 100 μM ADP-ribose.

on ADP-ribose-induced TRPM2 gating provides further evidence against direct or membrane-delimited mechanisms for activation of full-length TRPM2 channels. Furthermore, although the potential promiscuity of these reagents at the concentrations used in our experiments precludes any specific conclusions regarding their molecular target, their observed effects are consistent with their acting as structural mimics of NAD so as to blunt oxidative/nitrosative stress-induced accumulation of ADP-ribose via inhibition of NAD hydrolysis.

As a second approach to testing whether ADP-ribose accumulation was involved in oxidative/nitrosative stress-induced TRPM2 gating, we reasoned that enhancing the rate of degradation of ADP-ribose through the cytosolic expression of an enzyme that breaks it down should delay or suppress oxidative/nitrosative stress-induced TRPM2 activation. For this purpose, we generated a cell line, which constitutively expresses TRPM2, and which in addition has tetracycline-regulated expression of a non-compartmentalized form of the NUDT9 ADP-ribose pyrophosphatase (ADPRase), designated cytNUDT9. An important point when using NUDT9 as a tool in this manner is that experimental analysis of NUDT9 by two different laboratories indicates that its only significant physiological activity is toward ADP-ribose (15, 17, 34). As shown in Fig. 5, exposure of these cells to H_2O_2 or MNNG produces large calcium transients similar to those observed after inducible TRPM2 expression in HEK cells in Fig. 1 (Fig. 5, *A* and *B*, *dark traces*, compare with Fig. 1 and note that in the parental cell line for the stable TRPM2 transfectants, no oxidative/nitrosative stress-mediated calcium transients are observed at these oxidant exposure levels, data not shown). However, induction of cytNUDT9 through doxycycline treatment of the cells completely suppresses these transients (Fig. 5*C*, *light traces*, the diffuse fluorescence pattern observed for the cytNUDT9-GFP fusion protein demonstrates its lack of compartmentalization (the observed pattern is identical to that exhibited by GFP alone)). That cytNUDT9 expression is able to hinder the ability of cytosolic ADP-ribose to induce gating of TRPM2 was directly demonstrated by whole cell patch clamp experiments. In the absence of cytNUDT9 expression, TRPM2 gating is induced by cytosolic dialysis with 100 μM ADP-ribose with a short latency to a peak amplitude of ~10 nA of current (Fig. 5*D*). However, after cytNUDT9 expression, TRPM2 gating induced by cytosolic dialysis with 100 μM ADP-ribose occurs with a much longer latency and to a much smaller peak amplitude, directly demonstrating the ability of cytNUDT9 to hinder ADP-ribose-dependent gating of TRPM2. That these results do not reflect simply decreased surface expression of TRPM2 is demonstrated by identical experiments performed with 1 mM ADP-ribose (Fig. 5*E*), in which peak currents comparable with those in the absence of cytNUDT9 expression are observed to evolve with a much shorter latency, consistent with the increased ADP-ribose concentration overcoming the degradative ability of the overexpressed cytNUDT9. Because of its high specificity (15, 34), the capacity of overexpressed cytNUDT9 to hinder both oxidative/nitrosative stress-induced and direct ADP-ribose-induced TRPM2 gating (mediated by cytosolic dialysis of ADP-ribose in the patch clamp experiments) provides strong evidence that cytosolic-free ADP-ribose accumulation is required for oxidative/nitrosative stress-induced TRPM2 gating. An additional implication of the above results is that TRPM2 gating can be viewed as a surrogate marker of the cytosolic accumulation of free ADP-ribose. If one assumes that the dose-response curve of TRPM2 in whole cell

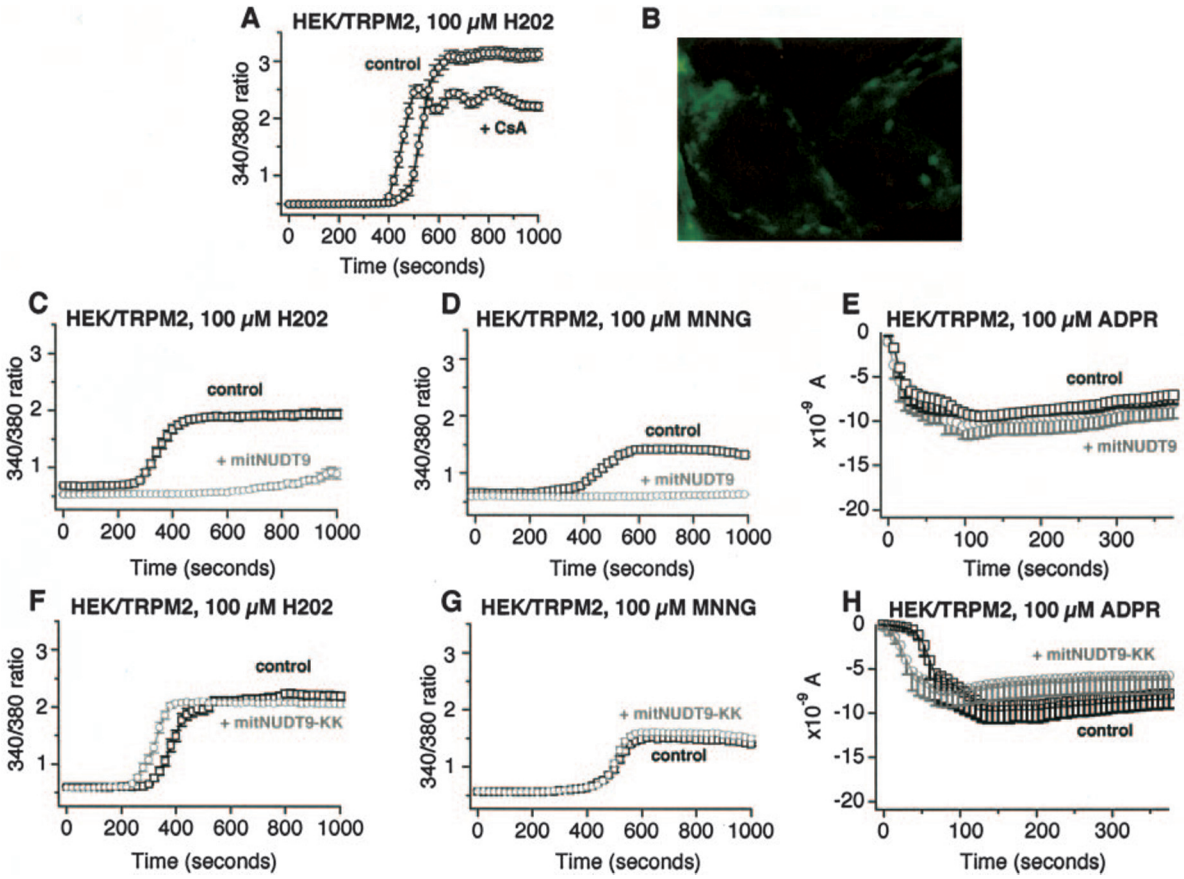

FIG. 6. **Overexpression of ADPRase activity in mitochondria suppresses TRPM2-dependent calcium transients induced by ROS or RNS.** *A*, cyclosporin A treatment does not affect oxidant-induced TRPM2-dependent calcium transients. TRPM2-expressing cells were stimulated with H_2O_2 in the absence (*control*) or presence (+ *CsA*) of cyclosporin A, and their cytosolic calcium responses were monitored via fura-2 imaging. *B*, subcellular distribution of mitNUDT9-tagged C-terminally with GFP. HEK-293 cells expressing TRPM2 were induced to express a cytNUDT9 fusion protein for 36 h. GFP fluorescence was imaged using 480 nm excitation and detection of 510–530 nm emission light on a Zeiss Axiovert 100 microscope. *C–E*, influence of mitNUDT9 on TRPM2-dependent calcium transients and ADP-ribose induced currents. Expression of mitNUDT9 suppresses H_2O_2- (*C*) and MNNG-(*D*) induced TRPM2-dependent calcium transients. Shown are calcium transients induced by 100 μM H_2O_2 or 100 μM MNNG, respectively, after induction of mitNUDT9 expression with doxycycline (*gray traces* with *circles*) or in the absence of mitNUDT9 expression (*black traces* with *squares*). Cytosolic calcium responses were monitored via fura-2 imaging. These studies were performed with 100 μM H_2O_2 and 100 μM MNNG as these stimulus concentrations did not induce detectable cell death over the course of a 1000-s imaging period as assessed by trypan blue staining (data not shown). *F*, mitNUDT9 expression does not affect patch clamp currents elicited by 100 μM ADP-ribose under unbuffered calcium conditions. Shown are currents elicited by 100 μM ADP-ribose after induction of mitNUDT9 expression with doxycycline (*gray traces* with *circles*) or in the absence of mitNUDT9 expression (*black traces* with *squares*). *F–H*, influence of mitNUDT9-KK on TRPM2-dependent calcium transients and ADP-ribose induced currents. Expression of mitNUDT9-KK does not affect H_2O_2- (*G*) or MNNG-(*H*) induced TRPM2-dependent calcium transients. Shown are calcium transients induced by 100 μM H_2O_2 or 100 μM MNNG, respectively, after induction of mitNUDT9-KK expression with doxycycline (*gray traces* with *circles*) or in the absence of mitNUDT9-KK expression (*black traces* with *squares*). These studies were performed with 100 μM H_2O_2 and 100 μM MNNG as these stimulus concentrations did not induce cell death over the course of a 1000-s imaging period as assessed by trypan blue staining (data not shown). *I*, mitNUDT9-KK expression does not significantly affect whole cell patch clamp currents elicited using 100 μM ADP-ribose under unbuffered calcium conditions. Shown are currents elicited by 100 μM ADP-ribose after induction of mitNUDT9-KK expression with doxycycline (*gray traces* with *circles*) or in the absence of mitNUDT9-KK expression (*black traces* with *squares*).

patch clamp experiments under conditions where calcium is left unbuffered can be extrapolated to intact cell conditions (15), then cytosolic-free ADP-ribose can be inferred to be accumulating to a level greater than ≈10 μM under our experimental oxidative/nitrosative stress conditions.

We next considered potential cellular sources of free ADP-ribose. Mitochondria contain millimolar levels of NAD and NADH (amounting to >50% of total cellular pyridine nucleotides (35, 36)), are a major site of endogenous NUDT9 ADPRase activity (17), and have been reported to hydrolyze NAD in response to oxidant exposure *in vitro* (37–39), providing a strong rationale for evaluating their role in oxidative/nitrosative stress-induced ADP-ribose production involved in TRPM2 gating. As NAD hydrolysis occurring upon oxidant exposure of mitochondria has been associated with mitochondrial permeability transition (MPT) (40), and MPT can be pharmacologically suppressed *in vitro* by the drug cyclosporin A (41), we evaluated TRPM2 gating in the presence and absence of cyclosporin A to determine whether mitochondrial MPT-associated NAD hydrolysis was contributing to the ADP-ribose accumulation responsible for oxidant-induced TRPM2 gating. (Fig. 6*A*). As can be seen, cyclosporin A did not suppress TRPM2 activation even when used at a concentration well above that shown to suppress MPT in isolated mitochondria, suggesting that MPT-associated NAD hydrolysis is not required for the accumulation of sufficient cytosolic ADP-ribose to induce TRPM2 gating, at least under these experimental conditions. This conclusion is further supported by the observation that treatment of our HEK-293 cells with 100 μM H_2O_2 did not induce detectable long term cell death under our culture conditions unless TRPM2 was expressed and activable (*e.g.* toxicity was noted if TRPM2 was present, but not if it was absent or if TRPM2 activation was blocked by cytNUDT9, data not shown), as would have been expected if sustained MPT were occurring. To

investigate whether oxidative/nitrosative stress exposure might induce ADP-ribose production by an alternative mitochondrial mechanism, we constructed a cell line analogous to that used in Fig. 5, but with inducible expression of the mitochondrially targeted isoform of NUDT9 (mitNUDT9, Fig. 6*B*, its high degree of compartmentalization is demonstrated; that this corresponds to specific mitochondrial localization of this form of NUDT9 has been previously demonstrated (17)). As can be seen in Fig. 6, *C* and *D*, this cell line produces a calcium transient in response to 100 μM H_2O_2 and 100 μM MNNG, and this calcium transient is substantially (H_2O_2) or completely (MNNG) suppressed by induction of mitNUDT9. Importantly, in contrast to expression of cytNUDT9, which delays TRPM2 activation induced by cytosolic dialysis of free ADP-ribose in whole cell patch clamp experiments, the expression of mitNUDT9 did not affect patch pipette ADP-ribose-induced gating of TRPM2 (Fig. 6*E*). This result is particularly important in that it indicates that mitNUDT9 expression does not affect ADP-ribose accumulation once the ADP-ribose has entered the cytosol and thus implicates mitochondria as a site of production of ADP-ribose responsible for oxidant-induced TRPM2 gating. Because expression of a mitochondrially targeted protein could conceivably produce a biological effect via competition for the mitochondrial protein import machinery, we further tested the specificity of the mitNUDT9 effect by generating a cell line expressing an inactive form of mitNUDT9 designated mitNUDT9-KK (17). As can be seen in Fig. 6, *F* and *G*, expression of this protein had no effect on the H_2O_2 or MNNG-induced calcium transients, and as expected, whole cell patch clamp experiments showed no effect on ADP-ribose-induced TRPM2 gating in the presence or absence of mNUDT9-KK (Fig. 6*H*). The expression levels of the mitNUDT9 and mitNUDT9-KK were also compared by Western blot and found to be identical, and mitNUDT9-KK had an identical specific mitochondrial distribution (data not shown), confirming that differences in expression level or targeting do not explain the differential effects on TRPM2 activation of the enzymatically active and inactive forms of mitNUDT9.

DISCUSSION

In summary, we present a structural model that indicates the presence of a binding cleft in the C-terminal NUDT9-H domain of TRPM2, which appears capable of interacting with ADP-ribose but not NAD, and a mutational structure/function analysis of TRPM2, which implicates this binding cleft in both ADP-ribose-induced and oxidative/nitrosative stress-induced TRPM2 gating. Based on these data, we tested the hypothesis that oxidative and nitrosative stress lead to the accumulation of ADP-ribose using pharmacological methods predicted to limit NAD hydrolysis to ADP-ribose, and molecular genetic methods to enhance ADP-ribose degradation in cytosolic or mitochondrial compartments. Together, the data from these studies indicate that accumulation of cytosolic ADP-ribose released from mitochondria is required for oxidative- and nitrosative-stress-induced gating of TRPM2 cation channels.

In addition to highlighting the likely structural similarities between NUDT9 and TRPM2, our structural model provides a context in which to interpret the observation that deletions in TRPM2 in the vicinity of residues 1292–1325 result in mutant TRPM2 channels with varying capacities to gate in response to ADP-ribose (Refs. 13 and 20 and this work). All of the described deletions involve a TRPM2 NUDT9-H region between residues 1290–1327 corresponding to a large external loop on the opposite side of the NUDT9-H from the ADP-ribose binding cleft. Channels with deletions encompassing up to residues 1290–1318 (29 residues) remain capable of gating in response to ADP-ribose, whereas those with deletions of 1292–1325 (34 residues), 1290–1327 (39 residues), and deletion of Asn^{1326} have lost the capacity to gate. In our NUDT9-H model, Asn^{1326} is at one end of this large external loop and is packed tightly against Trp^{1439}, which sits at the end of the central β sheet, β16, traversing the length of the NUDT9-H domain. Consequently, the loss of the Asn^{1326}-Trp^{1439} interaction via a deletion of residues 1290–1327 or the Asn^{1326} residue alone seems likely to substantially alter the ability of the NUDT9-H to fold properly, which would account for the lack of activity of both of these channels. The deletion of residues 1290–1318 would leave the Asn^{1326}-Trp^{1439} interaction intact as well as a residual amino acid sequence sufficient to produce a smaller loop that still appears to be capable of spanning the gap without inducing significant strain on Asn^{1326}-Trp^{1439} packing, which is consistent with this mutant or smaller deletions retaining normal or near normal function (20). In contrast, deletion of residues 1292–1325 does not appear to leave a sufficiently large peptide to bridge the resulting gap, suggesting that this channel would not be able to fold properly, consistent with its loss of capacity to gate in response to ADP-ribose. Overall, the above analysis suggests that a properly folded NUDT9-H domain is crucial for producing gateable TRPM2 channels. As deletion of the entire NUDT9-H domain strongly decreases TRPM2 labeling in surface biotinylation experiments (see Fig. 3*C*), an encompassing explanation for the observed behavior of the TRPM2 NUDT9-H deletion mutants would be that a properly folded NUDT9-H domain is required for TRPM2 surface trafficking. The role of the NUDT9-H domain in TRPM2 surface expression will therefore be an essential issue to investigate and account for in future analyses of TRPM2 structure/function relationships.

Our experimental observation that the TRPM2-RILRKK mutant channel is functional merits comment, as it also has significant implications regarding the role of the NUDT9-H in TRPM2 function. The preservation of both apparently normal oxidative/nitrosative stress-induced calcium transients and ADP-ribose-induced gating in whole cell patch clamp studies involving this channel, whose enzymatic activity is predicted to be markedly reduced relative to the wild type TRPM2, provides strong evidence that ADP-ribose enzymatic activity is not required for TRPM2 gating. This lends credence to the hypothesis that the NUDT9-H domain has been adapted by evolution primarily to function as an ADP-ribose binding domain. However, these results do not exclude that the small amount of ADP-ribose hydrolase activity possessed by wild type TRPM2 has a physiological role, as it is possible that more detailed single channel analyses will reveal alterations in more subtle aspects of TRPM2 gating, or that the enzymatic activity has a role in some other aspect of TRPM2 function.

The most significant conclusion to emerge from our analyses of oxidative/nitrosative-stress induced TRPM2 gating is that a biochemical pathway is present in mitochondria through which free ADP-ribose is generated and released to the cytosol in response to oxidative and nitrosative stress. However, the nature of this biochemical pathway is presently unclear. Two lines of evidence suggest a potential role of PARP-1, a widely studied DNA damage-activated member of the poly(ADP-ribose) polymerase family, in oxidative/nitrosative stress-induced TRPM2 gating: 1) TRPM2 gating is induced by concentrations of H_2O_2 and MNNG widely used to induce PARP-1 activation (25, 42, 43), and 2) we and others have observed that small molecules known to inhibit PARP-1 have the capacity to block oxidant-mediated TRPM2 gating (this work and Ref. 44). However, although evidence has been presented to indicate

that PARP-1 is present in mitochondria (43), H_2O_2 and MNNG have also both been suggested to have direct effects on mitochondria (38, 45), such that the interpretation of their capacity to induce TRPM2 gating as dependent solely on their capacity to induce DNA damage and activate PARP-1 may not be justified. In addition, PARP-1 inhibitors are known to be promiscuous within the PARP family because of their structural mimicry of nicotinamide (24, 33, 46), and the concentrations required to inhibit oxidant-mediated TRPM2 gating are well above those required to inhibit PARP-1 *in vitro*, precluding an unambiguous interpretation of the *in cellulo* or *in vivo* targets of these compounds. Finally, it is not obvious, at least to these authors, why PARP-1 activation should be connected to activation of a plasma membrane cation channel. Therefore, a definitive identification of the biochemical mechanisms through which oxidative/nitrosative stress induces mitochondrial ADP-ribose production is an important topic for future investigation and offers the possibility of producing novel insights into both mitochondrial physiology and the biological role of TRPM2.

An intriguing question stemming from our results is whether the mitochondrial mechanisms involved in the production of free ADP-ribose have other physiological functions. Oxidant-induced TRPM2 gating is supported by diverse vertebrate cell types, including many that do not normally express TRPM2 channels (*e.g.* our HEK cell lines used here and DT40 B-lymphocytes),[2] suggesting that oxidant-induced mitochondrial ADP-ribose release is a fundamental aspect of mitochondrial metabolism in vertebrate cells and not simply an adaptation to induce TRPM2 gating (13–16, 18, 28, 47–49). In this regard, *Drosophila melanogaster* and *Caenorhabditis elegans*, both of which lack orthologues of TRPM2, both also possess proteins highly homologous to NUDT9, suggesting that they also possess a biochemical pathway that generates ADP-ribose. However, no NUDT9 homologue is present in either of the unicellular eukaryotes *Saccharomyces cerevisiae* or *Schizosaccharomyces pombe*. We speculate that multicellular organisms may have evolved the biochemical machinery required for oxidative/nitrosative stress-induced mitochondrial ADP-ribose production, because it serves as an acutely beneficial biochemical compensation during such stress situations, or because mitochondrial ADP-ribose production and release has alternative second messenger/signaling roles of relevance to the function of multicellular organisms.

A final issue of potential relevance is that of pathological effects associated with free ADP-ribose accumulation to the 10s of micromolar concentration range suggested by its dose-response relationship for TRPM2 gating. Mitochondrial ROS production has been proposed as a central component of the pathophysiology associated with diabetes and aging, in part because of its capacity to induce the accumulation of advanced glycation end products (reviewed in Ref. 50). Among pentose-reducing sugars produced by cellular metabolism, ADP-ribose has been shown to have the highest propensity to form advanced glycation end products, even at low 10s of micromolar concentrations (51, 52). In addition, ADP-ribose is a known inhibitor of glyceraldehyde-3-phosphate dehydrogenase (53, 54), inhibition of which is thought to shunt triose phosphates into several biochemical pathways associated with oxidative cell damage, including that associated with advanced glycation end-product formation (55, 56). Therefore, accumulation of free ADP-ribose may have an important role in the mechanisms through which mitochondrial or other sources of oxidative stress leads to metabolic derangements associated with disease or aging.

Acknowledgment—We thank Reinhold Penner for helpful comments and discussion.

REFERENCES

1. Chiarugi, P., and Cirri, P. (2003) *Trends Biochem. Sci.* **28,** 509–514
2. Dickinson, D. A., and Forman, H. J. (2002) *Ann. N. Y. Acad. Sci.* **973,** 488–504
3. Filomeni, G., Rotilio, G., and Ciriolo, M. R. (2002) *Biochem. Pharmacol.* **64,** 1057–1064
4. Finkel, T. (2003) *Curr. Opin. Cell Biol.* **15,** 247–254
5. Giles, N. M., Watts, A. B., Giles, G. I., Fry, F. H., Littlechild, J. A., and Jacob, C. (2003) *Chem. Biol.* **10,** 677–693
6. Grant, C. M. (2001) *Mol. Microbiol.* **39,** 533–541
7. Kamata, H., and Hirata, H. (1999) *Cell. Signal.* **11,** 1–14
8. Klatt, P., and Lamas, S. (2000) *Eur. J. Biochem.* **267,** 4928–4944
9. Mikkelsen, R. B., and Wardman, P. (2003) *Oncogene* **22,** 5734–5754
10. Mongkolsuk, S., and Helmann, J. D. (2002) *Mol. Microbiol.* **45,** 9–15
11. Paget, M. S., and Buttner, M. J. (2003) *Annu. Rev. Genet.* **37,** 91–121
12. Schafer, F. Q., and Buettner, G. R. (2001) *Free Radic. Biol. Med.* **30,** 1191–1212
13. Wehage, E., Eisfeld, J., Heiner, I., Jungling, E., Zitt, C., and Luckhoff, A. (2002) *J. Biol. Chem.* **277,** 23150–23156
14. Hara, Y., Wakamori, M., Ishii, M., Maeno, E., Nishida, M., Yoshida, T., Yamada, H., Shimizu, S., Mori, E., Kudoh, J., Shimizu, N., Kurose, H., Okada, Y., Imoto, K., and Mori, Y. (2002) *Mol. Cell* **9,** 163–173
15. Perraud, A. L., Fleig, A., Dunn, C. A., Bagley, L. A., Launay, P., Schmitz, C., Stokes, A. J., Zhu, Q., Bessman, M. J., Penner, R., Kinet, J. P., and Scharenberg, A. M. (2001) *Nature* **411,** 595–599
16. Perraud, A. L., Schmitz, C., and Scharenberg, A. M. (2003) *Cell Calcium* **33,** 519–531
17. Perraud, A. L., Shen, B., Dunn, C. A., Rippe, K., Smith, M. K., Bessman, M. J., Stoddard, B. L., and Scharenberg, A. M. (2003) *J. Biol. Chem.* **278,** 1794–1801
18. Sano, Y., Inamura, K., Miyake, A., Mochizuki, S., Yokoi, H., Matsushime, H., and Furuichi, K. (2001) *Science* **293,** 1327–1330
19. Jacobson, E. L., Cervantes-Laurean, D., and Jacobson, M. K. (1997) *Adv. Exp. Med. Biol.* **419,** 371–379
20. Kuhn, F. J., and Luckhoff, A. (2004) *J. Biol. Chem.* **279,** 46431–46437
21. Fiser, A., and Sali, A. (2003) *Methods Enzymol.* **374,** 461–491
22. Fiser, A., and Sali, A. (2003) *Bioinformatics* **19,** 2500–2501
23. Brunger, A. T., Adams, P. D., Clore, G. M., DeLano, W. L., Gros, P., Grosse-Kunstleve, R. W., Jiang, J. S., Kuszewski, J., Nilges, M., Pannu, N. S., Read, R. J., Rice, L. M., Simonson, T., and Warren, G. L. (1998) *Acta Crystallogr. Sect. D Biol. Crystallogr.* **54,** 905–921
24. Ferraris, D., Ko, Y. S., Pahutski, T., Ficco, R. P., Serdyuk, L., Alemu, C., Bradford, C., Chiou, T., Hoover, R., Huang, S., Lautar, S., Liang, S., Lin, Q., Lu, M. X., Mooney, M., Morgan, L., Qian, Y., Tran, S., Williams, L. R., Wu, Q. Y., Zhang, J., Zou, Y., and Kalish, V. (2003) *J. Med. Chem.* **46,** 3138–3151
25. Yu, S. W., Wang, H., Poitras, M. F., Coombs, C., Bowers, W. J., Federoff, H. J., Poirier, G. G., Dawson, T. M., and Dawson, V. L. (2002) *Science* **297,** 259–263
26. Cooper, C. E., Patel, R. P., Brookes, P. S., and Darley-Usmar, V. M. (2002) *Trends Biochem. Sci.* **27,** 489–492
27. Di Simplicio, P., Franconi, F., Frosali, S., and Di Giuseppe, D. (2003) *Amino Acids (Vienna)* **25,** 323–339
28. Shen, B. W., Perraud, A. L., Scharenberg, A., and Stoddard, B. L. (2003) *J. Mol. Biol.* **332,** 385–398
29. Rechsteiner, M., Hillyard, D., and Olivera, B. M. (1976) *J. Cell. Physiol.* **88,** 207–217
30. Hillyard, D., Rechsteiner, M., Manlapaz-Ramos, P., Imperial, J. S., Cruz, L. J., and Olivera, B. M. (1981) *J. Biol. Chem.* **256,** 8491–8497
31. Hillyard, D., Rechsteiner, M. C., and Olivera, B. M. (1973) *J. Cell. Physiol.* **82,** 165–179
32. Kinoshita, T., Nakanishi, I., Warizaya, M., Iwashita, A., Kido, Y., Hattori, K., and Fujii, T. (2004) *FEBS Lett.* **556,** 43–46
33. Ferraris, D., Ficco, R. P., Dain, D., Ginski, M., Lautar, S., Lee-Wisdom, K., Liang, S., Lin, Q., Lu, M. X., Morgan, L., Thomas, B., Williams, L. R., Zhang, J., Zhou, Y., and Kalish, V. J. (2003) *Bioorg. Med. Chem.* **11,** 3695–3707
34. Lin, S., Gasmi, L., Xie, Y., Ying, K., Gu, S., Wang, Z., Jin, H., Chao, Y., Wu, C., Zhou, Z., Tang, R., Mao, Y., and McLennan, A. G. (2002) *Biochim. Biophys. Acta* **1594,** 127–135
35. Livingston, B. E., Altschuld, R. A., and Hohl, C. M. (1996) *Pediatr. Res.* **40,** 59–65
36. Tischler, M. E., Hecht, P., and Williamson, J. R. (1977) *Arch. Biochem. Biophys.* **181,** 278–293
37. Schweizer, M., Schlegel, J., Baumgartner, D., and Richter, C. (1993) *Biochem. Pharmacol.* **45,** 641–646
38. Richter, C. (1984) *Methods Enzymol.* **105,** 435–441
39. Richter, C., Theus, M., and Schlegel, J. (1990) *Biochem. Pharmacol.* **40,** 779–782
40. Crompton, M., Ellinger, H., and Costi, A. (1988) *Biochem. J.* **255,** 357–360
41. Kroemer, G. (2003) *Curr. Med. Chem.* **10,** 1469–1472
42. Hour, T. C., Shiau, S. Y., and Lin, J. K. (1999) *Toxicol. Lett.* **110,** 191–202
43. Du, L., Zhang, X., Han, Y. Y., Burke, N. A., Kochanek, P. M., Watkins, S. C., Graham, S. H., Carcillo, J. A., Szabo, C., and Clark, R. S. (2003) *J. Biol. Chem.* **278,** 18426–18433
44. Fonfria, E., Marshall, I. C., Benham, C. D., Boyfield, I., Brown, J. D., Hill, K., Hughes, J. P., Skaper, S. D., and McNulty, S. (2004) *Br. J. Pharmacol.* **143,** 186–192

[2] A. L. Perraud, C. Takanishi, and A. M. Scharenberg, unpublished data.

45. Dodoni, G., Canton, M., Petronilli, V., Bernardi, P., and Di Lisa, F. (2004) *Biochim. Biophys. Acta* **1658,** 58–63
46. Ruf, A., de Murcia, G., and Schulz, G. E. (1998) *Biochemistry* **37,** 3893–3900
47. Kraft, R., Grimm, C., Grosse, K., Hoffmann, A., Sauerbruch, S., Kettenmann, H., Schultz, G., and Harteneck, C. (2004) *Am. J. Physiol.* **286,** C129–C137
48. Inamura, K., Sano, Y., Mochizuki, S., Yokoi, H., Miyake, A., Nozawa, K., Kitada, C., Matsushime, H., and Furuichi, K. (2003) *J. Membr. Biol.* **191,** 201–207
49. Heiner, I., Eisfeld, J., Halaszovich, C. R., Wehage, E., Jungling, E., Zitt, C., and Luckhoff, A. (2003) *Biochem. J.* **371,** 1045–1053
50. Brownlee, M. (2001) *Nature* **414,** 813–820
51. Cervantes-Laurean, D., Jacobson, E. L., and Jacobson, M. K. (1996) *J. Biol. Chem.* **271,** 10461–10469
52. Booth, A. A., Khalifah, R. G., Todd, P., and Hudson, B. G. (1997) *J. Biol. Chem.* **272,** 5430–5437
53. Eby, D., and Kirtley, M. E. (1971) *Biochemistry* **10,** 2677–2682
54. Shen, Y. Q., Song, S. Y., and Lin, Z. J. (2002) *Acta Crystallogr. Sect. D Biol. Crystallogr.* **58,** 1287–1297
55. Hammes, H. P., Du, X., Edelstein, D., Taguchi, T., Matsumura, T., Ju, Q., Lin, J., Bierhaus, A., Nawroth, P., Hannak, D., Neumaier, M., Bergfeld, R., Giardino, I., and Brownlee, M. (2003) *Nat. Med.* **9,** 294–299
56. Babaei-Jadidi, R., Karachalias, N., Ahmed, N., Battah, S., and Thornalley, P. J. (2003) *Diabetes* **52,** 2110–2120
57. Niknahad, H., and O'Brien, P. J. (1995) *Xenobiotica* **25,** 91–101